Three-Dimensional Computation of Light Scattering From Cells

Andrew Dunn and Rebecca Richards-Kortum

***Abstract*— Using the finite-difference time-domain method, three-dimensional scattering patterns are computed for cells containing multiple organelles. The scattering cross section and average cosine of the scattering angle are computed for cells as a function of volume fraction of melanin granules and mitochondria. Results show that small organelles play a significant role in light scattering from cells, and the volume fraction of organelles affects both the total amount of scattered light and the angular distribution of scattered light.**

I. Introduction

RECENTLY, the potential of diagnostic optical imaging has generated considerable interest in the optical properties of tissues and cells at near infrared wavelengths, where scattering is dominant over absorption. Both direct and indirect imaging applications rely on the scattering properties of tissue to infer information about the physiological state of the tissue. Confocal microscopy [1] and optical coherence tomography (OCT) imaging [2], which are direct imaging techniques, provide high-resolution images of human tissue *in vivo* by constructing a three-dimensional (3-D) backscattering map that is a direct image of tissue morphology. Indirect techniques, such as near infrared spectroscopy techniques, relate changes in the amount of diffusely backscattered light to the optical properties of tissue [3], [4]. Attempts to relate directly or indirectly measured changes in tissue scattering to cellular physiological differences, such as those between normal and cancerous cells, have been difficult since the mechanisms by which cellular changes affect light scattering are not fully understood. This is primarily due to the difficulty in describing scattering at the cellular level since cells are complex structures with a spatially varying index of refraction.

There are two important parameters that influence the scattering properties of tissue: tissue morphology and biochemistry. Tissue morphology, or the relative size of organelles and cells with respect to the wavelength of light, affects the angular distribution of the scattered light. Generally, a tissue component whose size is small compared to the wavelength will scatter light more isotropically than larger components, but the total amount of scattered light will be less for the smaller component due to its smaller size. The index of refraction of each component is determined by the biochemical makeup of the tissue and will influence the amplitude of the scattered light. A larger difference in the index of refraction between a cell component and its surrounding will result in increased scattering. A better understanding of the relationship between the biochemical and morphological structure of cells and light scattering will aid in the development of diagnostic applications.

Mie theory has been used to approximate tissue scattering at the cellular level by assuming cells are homogeneous spheres of a single size [5]. While Mie theory has been successful in describing light propagation in bulk tissue, it cannot describe the light interaction with complex structures such as individual cells containing multiple organelles. Mie theory can describe the scattering of individual spherical organelles, but it cannot account for a combination of organelles within a cell.

To account for scattering that arises from inhomogeneous objects of arbitrary shape, a more complex model is needed. In this paper we present the application of the finite-difference time-domain (FDTD) method to model light scattering from cells containing multiple organelles. The FDTD technique is a powerful computational method that is a full vector, 3-D solution of Maxwell's equations. Complex objects of any dielectric structure can be modeled, and the scattered electromagnetic fields can be calculated for cells containing a nucleus and other organelles. The angular distribution of scattered light, or scattering pattern, anisotropy value, g, and scattering cross section are computed. Simulations of cells containing various volume fractions of various organelles are performed to assess the effect of these organelles on tissue scattering. Specifically, mitochondria and melanin are studied since it has been suggested that each plays an important role in tissue scattering. In the first section the FDTD method is briefly outlined, and sufficient detail is provided to implement the technique for cell scattering calculations, then some example results are presented.

II. FDTD Method

A. Yee's Algorithm

The FDTD method, first described by Yee [6], is a direct solution of Maxwell's equations in the time domain. It has been used in a wide range of applications including electromagnetic absorption of tissue in hyperthermia [7], scattering cross-section calculations of arbitrary objects [8], scattering from frequency-dependent materials [9], as well as many other applications [10].

Manuscript received September 26, 1996. This work was supported in part by the National Science Foundation under Grant BCS-9 157 202 and the Center for High Performance Computing at the University of Texas.

The authors are with the Biomedical Engineering Program, Department of Electrical and Computer Engineering, University of Texas, Austin, TX 78731 USA.

Publisher Item Identifier S 1077-260X(96)09666-9.

Yee's algorithm begins with Maxwell's two curl equations

$$\nabla \times \vec{E} = -\mu \frac{\partial \vec{H}}{\partial t} \tag{1}$$
$$\nabla \times \vec{H} = \sigma \vec{E} + \epsilon \frac{\partial \vec{E}}{\partial t}$$

and discretizes them in space and time, resulting in a set of six explicit finite-difference equations. The electric and magnetic fields are spatially and temporally offset on a 3-D grid. Examples of the finite-difference equations for the x component of the electric field, E_x, and y component of the magnetic field, H_y, are

$$\begin{aligned} E_x^{n+1}(i+1/2,j,k) &= E_x^n(i+1/2,j,k) + \frac{dt}{\epsilon(i+1/2,j,k)dx} \\ &\quad \times [H_z^{n+1/2}(i+1/2,j+1/2,k) \\ &\quad - H_z^{n+1/2}(i+1/2,j-1/2,k) \\ &\quad + H_y^{n+1/2}(i+1/2,j,k-1/2) \\ &\quad - H_y^{n+1/2}(i+1/2,j,k+1/2)] \end{aligned} \tag{2}$$

$$\begin{aligned} H_y^{n+1/2}(i+1/2,j,k+1/2) &= H_y^{n-1/2}(i+1/2,j,k+1/2) \\ &\quad + \frac{dt}{\mu dx}[E_z^n(i+1,j,k+1/2) \\ &\quad - E_z^n(i,j,k+1/2) \\ &\quad + E_x^n(i+1/2,j,k) \\ &\quad - E_x^n(i+1/2,j,k+1)]. \end{aligned} \tag{3}$$

Similar equations exist for the remaining electric and magnetic field components [11]. In (2) and (3), (i,j,k) is the location of a grid point, and dx and dt are the spatial and temporal step sizes. The time step is indicated by the superscript n, and ϵ and μ are the electric permittivity and magnetic permeability, respectively. The six finite-difference equations are stepped in time, alternately updating the electric and magnetic field components at each grid point.

To simulate propagation in an unbounded medium, special boundary conditions must be applied to the tangential electric field components along the edges of the computational boundaries at each time step, as indicated in Fig. 1. A variety of boundary conditions exist [12] and are usually based on either a solution of the wave equation [13], [14] to prevent artificial reflections at the edges of the computational domain or an artificial material absorber around the edges to effectively damp out any reflections [15]. The second-order Mur absorbing boundary condition was used in this paper [13].

The incident wave is not included in the finite-difference equations for the field components and therefore is applied separately. The total field/scattered field formulation [16] can be used to propagate a variety of excitation waveforms, including a continuous sinusoid and a Gaussian pulse. In the interior of the computational domain, the total fields (incident and scattered) are calculated, while around the edges the scattered and incident fields are treated separately. In this paper a sinusoidal plane wave source of the form $\sin(\omega t)$ is propagated in the $+z$ direction.

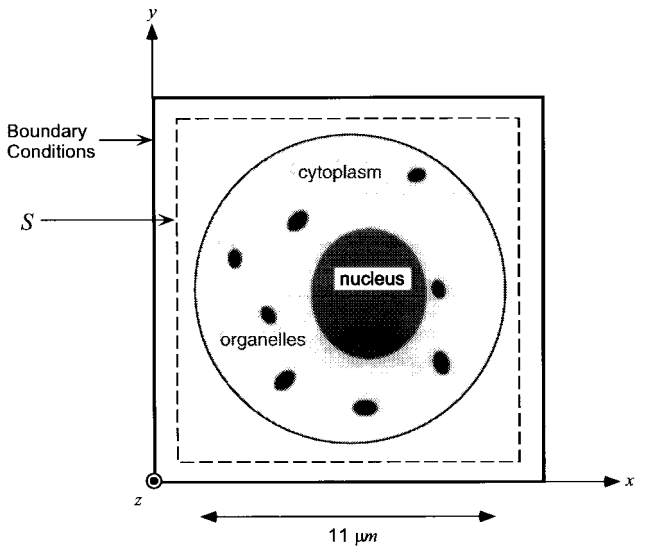

Fig. 1. Geometry of the FDTD simulation demonstrating how the cell is constructed by assigning each component a different index of refraction.

As illustrated in Fig. 1, the cell is constructed within the grid by assigning a value of the permittivity to each region, or organelle, within the cell. In this way, the cell is constructed as a dielectric object that can have any number of components of varying shapes and sizes.

The total size of each problem is limited, however, by computational considerations since the grid spacing dx must be less than $\lambda/10$ [11]. This is due to the discretization of the fields, and step sizes greater than this lead to unstable results. For each simulation, values of the six field components and permittivity must be stored in memory at each point in the computational domain. Thus the size of the computational domain, and therefore storage requirements, are dictated by the wavelength and size of the object. In three dimensions, even moderately sized problems will exhaust the capabilities of current personal computers. However, the FDTD method is well suited for parallel processing [17], making 3-D problems more tractable.

B. Far-Field Transform

The FDTD method computes the fields in a region around the cell that lies in the near field. To determine the far-field scattering pattern, the near-field data can be transformed to the far field by weighting it with the free-space Green's function and integrating over a surface S, surrounding the cell (Fig. 1) [8], [18].

The near-field time-domain values are first converted to the frequency-domain values with a discrete Fourier transform [19], and the equivalent electric and magnetic surface current densities, J_s and M_s, are defined on the surface S as [20]

$$\vec{J}_s(\vec{r}\,') = \hat{n} \times \vec{H} \tag{4}$$
$$\vec{M}_s(\vec{r}\,') = -\hat{n} \times \vec{E}$$

where $\vec{r}\,'$ is a point on S and $\hat{n}$ is a unit vector normal to S, where the origin of the far-field transform is located in the

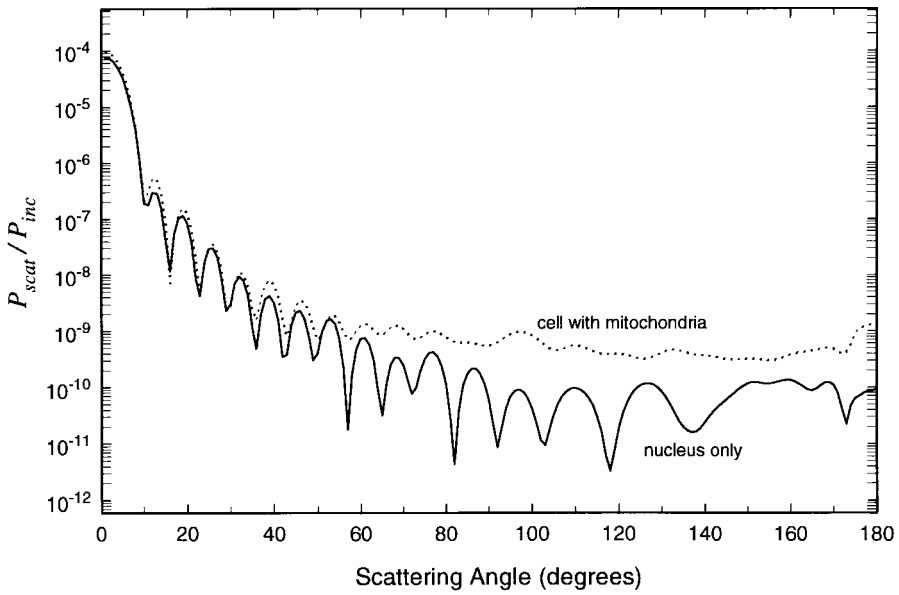

Fig. 2. Scattering patterns for a cell with only a nucleus and cytoplasm (solid line) and a cell with mitochondria [8.5% volume fraction (dotted line)].

center of the grid. The vector potentials A and F are computed by numerically integrating J_s and M_s over the surface S

$$\vec{A} = \frac{\mu_o e^{-jkr}}{4\pi r} \iint_S \vec{J}_s e^{jkr' \cos\psi}\, ds' \qquad (5)$$
$$\vec{F} = \frac{\epsilon_o e^{-jkr}}{4\pi r} \iint_S \vec{M}_s e^{jkr' \cos\psi}\, ds'$$

where r is a point in the far field and ψ is the angle between $\vec{r}$ and $\vec{r}\,'$. The far-field electric and magnetic field components, in spherical coordinates, are then given by

$$E_\theta = -j\omega(A_\theta + \eta_o F_\phi) \qquad (6)$$
$$E_\phi = -j\omega(A_\phi - \eta_o F_\theta)$$
$$H_\theta = \frac{j\omega}{\eta}(A_\phi - \eta_o F_\theta)$$
$$H_\phi = -\frac{j\omega}{\eta}(A_\theta + \eta_o F_\phi)$$

where $\eta = \sqrt{\mu/\epsilon}$. The far-field scattering pattern $F_s(\theta, \phi)$ is defined by

$$F_s(\theta,\phi) = \frac{1}{2}\Re\left(E_\theta H_\phi^*\right) + \frac{1}{2}\Re(-E_\phi H_\theta^*) \qquad (7)$$

where θ and ϕ are the angles measured from the z and x axes, respectively, in spherical coordinates. Physically, this represents the scattered intensity at any point in the far field. Other parameters such as the anisotropy and scattering cross section can be computed from the scattering pattern $F_s(\theta, \phi)$ (see Section IV).

III. Simulation Parameters

An FDTD code was written to compute the far-field scattering pattern of cells containing multiple organelles. In Fig. 1 a cross section of a typical cell is shown, where the shaded regions represent different values of permittivity, or index of refraction. There have been few published reports of the index of refraction of cells and organelles, and the values listed in Table I were taken from the literature and used in these simulations. The cell shown in Fig. 1 is ellipsoidal with a mean diameter of approximately 11 μm and the diameter of the nucleus is 3 μm, while the diameter of organelles, such as mitochondria, is uniformly distributed between 0.4 and 1 μm.

TABLE I
Index of Refraction Values Used in the FDTD Simulation

Cell Component	Index of Refraction	Reference
extracellular fluid	1.35	[28]
cytoplasm	1.37	[29]
nucleus	1.39	[29]
mitochondria	1.42	[30]
melanin	1.7	[31]

The simulation program was verified by computing the scattering pattern of homogeneous spheres ranging in diameter from 1 to 12 μm and comparing the results to Mie theory. The grid spacing in the simulations was $\lambda/20$ ($\lambda = 900$ nm) and a sinusoidal source, propagating in the $+z$ direction, was stepped in time until sinusoidal steady state of the scattered fields was reached, which typically required 3 to 4 passes through the grid. After completion of the time stepping, the scattering pattern, $F_s(\theta, \phi)$, was computed in one-degree increments for both θ and ϕ. Simulations were run on a Cray J90 computer, and each simulation typically required approximately 100 Mword of storage and 30 min of system CPU time for a 12-μm diameter object. The FDTD computed patterns agreed with the Mie theory patterns to within 1%–2% at all angles.

IV. Results

The scattering patterns for two cells are plotted in Fig. 2. The lower curve is the pattern for a cell with only a nucleus, while the other is for the same cell containing a nucleus and mitochondria with a volume fraction of 8.5%. The scattering pattern $F_s(\theta, \phi)$, has been averaged over the azimuthal angle

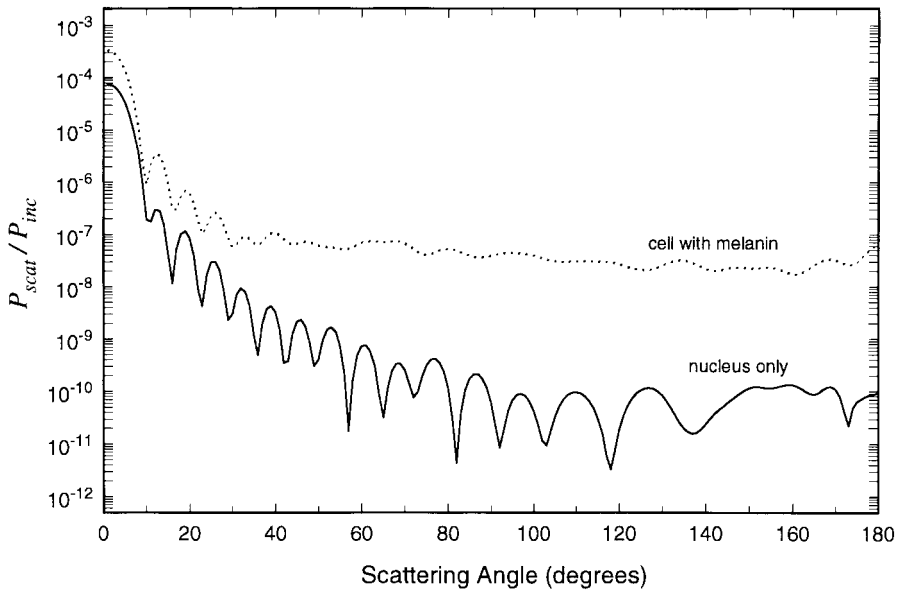

Fig. 3. Scattering patterns for a cell with only a nucleus and cytoplasm (solid line) and a cell with melanin [8.5% volume fraction (dotted line)].

and is therefore only a function of θ

$$F(\theta) = \frac{1}{2\pi} \int_0^{2\pi} F_s(\theta, \phi) d\phi. \tag{8}$$

The pattern is highly peaked in the forward direction, and the largest differences in amplitude between the two cells occur at angles above 90°. Below 90° the relative difference in amplitude is less pronounced.

In Fig. 3 the scattering patterns $F(\theta)$, for a cell with a nucleus only and a cell containing a nucleus and melanin with a volume fraction of 8.5%, are plotted. There is a significant increase in the amount of scatter at all angles relative to the cell without melanin.

To investigate the effect of the nucleus, the scattering patterns of a cell with and without a nucleus were compared (data not shown). There was little difference in the patterns except for a slight increase in amplitude at small angles ($<$ 10°). To compare the relative contributions of the nucleus and small organelles, the scattering patterns of a cell containing organelles and a nucleus, and a cell containing only organelles were compared. There is very little difference in the two patterns indicating that at near infrared wavelengths, small organelles play a more important role than the nucleus in scattering from a cell, and the effect of the nucleus on the scattering patterns for a cell with organelles is overshadowed by the scatter due to the organelles.

The Henyey–Greenstein phase function [21] is often used to characterize the angular distribution of scattered light by tissue and is characterized by the average cosine of the scattering angle g. Since the Henyey–Greenstein phase function is a probability density function, it is normalized to an area of one. To compare the computed scattering pattern to the Henyey–Greenstein phase function $p_{hg}(\theta)$, the scattering pattern was normalized to obtain a phase function

$$p(\theta) = \frac{F(\theta)}{\int_0^{\pi} F(\theta) \sin\theta d\theta}. \tag{9}$$

The average cosine g, of $p(\theta)$, was then computed

$$g = \int_0^{\pi} p(\theta) \cos\theta \sin\theta d\theta. \tag{10}$$

This value of g was then used for the Henyey–Greenstein phase function to compare the phase functions. Fig. 4(a) and (b) shows the comparison of the Henyey–Greenstein and computed phase functions for the cell containing mitochondria [Fig. 4(a)] and melanin [Fig. 4(b)]. The value of g for the cell containing mitochondria is 0.992, indicating almost complete forward scatter. The Henyey–Greenstein phase function for $g = 0.992$ shows significant differences from the cell phase function at almost all angles. In the cell with melanin [Fig. 4(b)], the value of g is smaller (0.944) and the Henyey–Greenstein phase function matches somewhat better, although there are still significant differences. The lower g value is the result of increased scattering at higher angles (Fig. 3).

The volume fraction of a particular organelle in cells will vary depending on tissue type. To investigate the effect of organelle volume fraction on scattering, the average cosine g and the scattering cross section C were computed for cells containing differing amounts of organelles. The scattering cross section was computed by integrating the scattering pattern over all angles

$$C = \int_0^{2\pi} \int_0^{\pi} F_s(\theta, \phi) \sin\theta d\theta d\phi. \tag{11}$$

In Fig. 5, C and g are plotted as a function of organelle volume fraction for organelles representing mitochondria. When

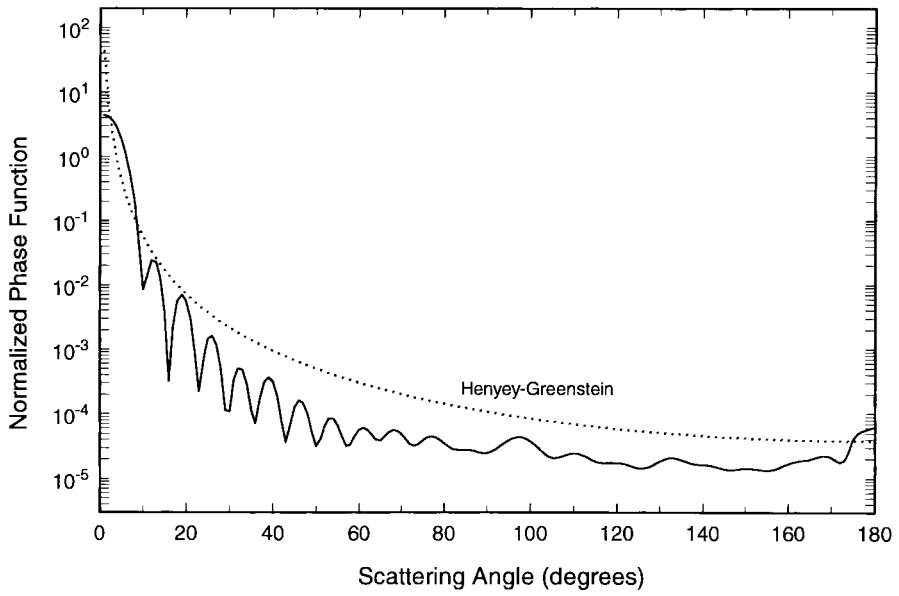

(a)

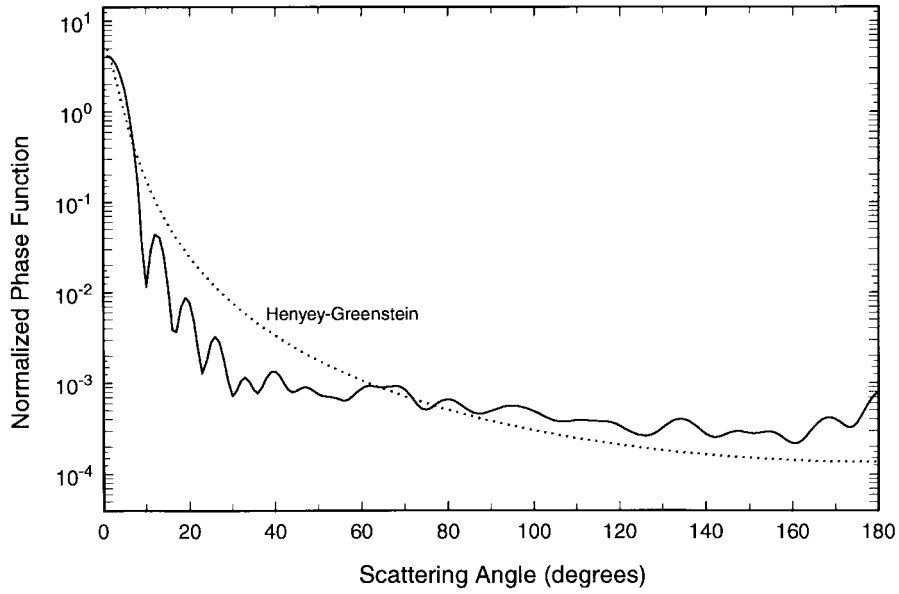

(b)

Fig. 4. Comparison of the Henyey–Greenstein phase function and the FDTD computed phase functions. (a) Cell with mitochondria (8.5% volume fraction). (b) Cell with melanin (8.5% volume fraction).

the organelle volume fraction is zero, the cell consists only of a nucleus and cytoplasm. The scattering cross section increases with organelle volume fraction, while the anisotropy value decreases, indicating that the organelles contribute to high angle scattering. In Fig. 6, the scattering cross section and anisotropy are plotted for increasing amounts of melanin within the cell. The scattering cross section increases with volume fraction, but the anisotropy remains relatively constant with increasing volume fraction after an initial decrease.

V. Discussion

The scattering pattern of tissue structures, such as cells, is important to understand because it contains information about both the amplitude and angular distribution of scattered light. Recently, it was demonstrated that the shape of the phase function can play a significant role in reflectance measurements when the source and detector are positioned close to each other [22]. While Mie theory can provide some insight into the scattering from cells, it cannot predict the influence of organelles on the scattering patterns of cells. In Fig. 2 the major difference in the scattering patterns between a cell with and without organelles lies at angles greater than 90°. At angles up to about 50° the patterns have the same basic shape, indicating that the cytoplasm, or overall cell size and shape, determines the forward scattering properties. At higher angles, the role of the small organelles is more pronounced, which could be predicted qualitatively since they are small

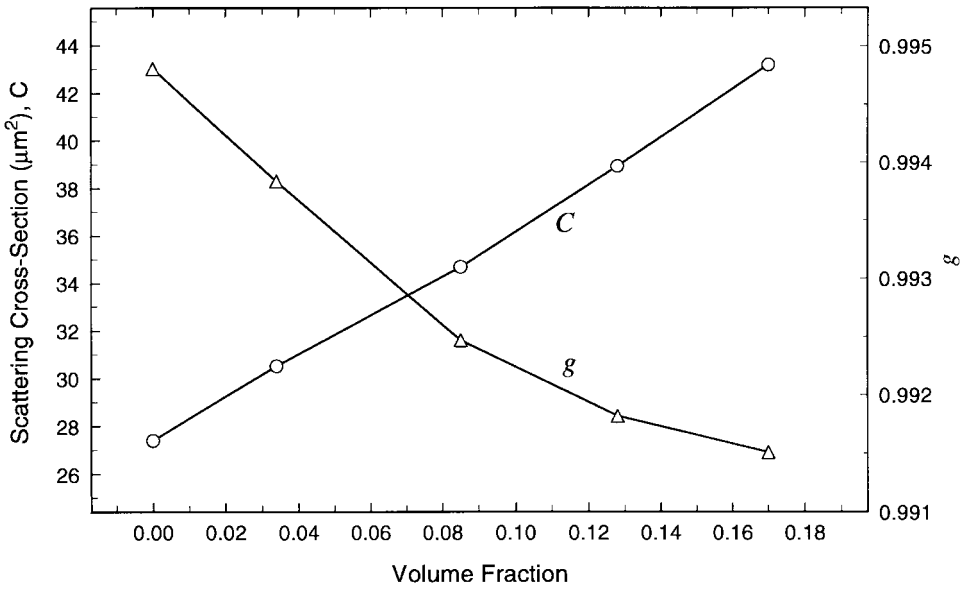

Fig. 5. Scattering cross section, C, and anisotropy value, g, as a function of organelle volume fraction ($n_{rel} = 1.03$).

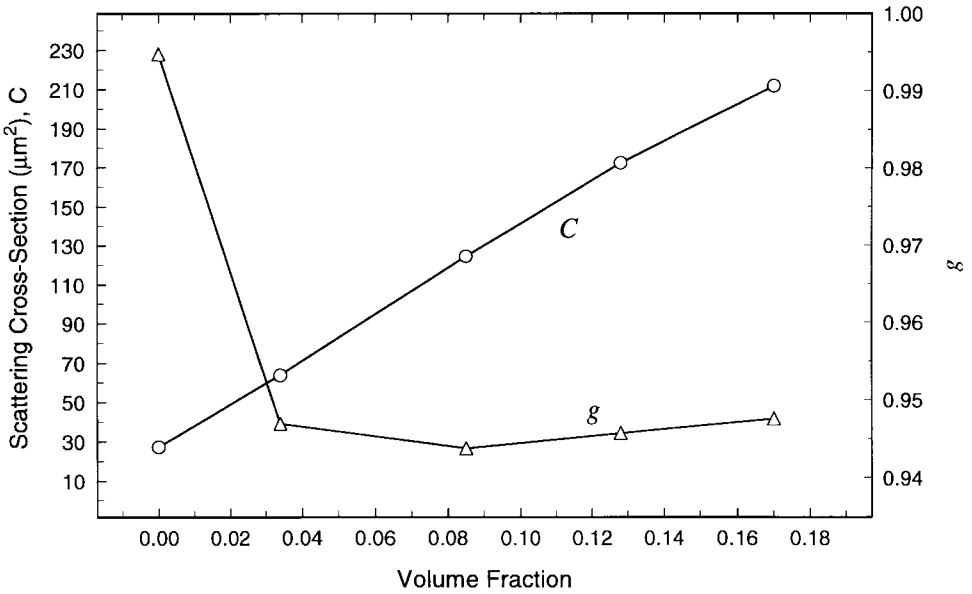

Fig. 6. Scattering cross section, C, and anisotropy value, g, as a function of melanin volume fraction.

relative to the wavelength and will act as isotropic scatterers. To predict the increase in high angle scatter quantitatively, however, the electromagnetic fields must be calculated.

The macroscopic scattering coefficient μ_s due to a collection of cells can be estimated from the scattering cross section C by [23]

$$\mu_s = \frac{\phi(1-\phi)}{V} C \tag{12}$$

where ϕ is the volume fraction of the cells relative to the whole tissue and V is the volume of a single cell. If we assume that the cells occupy 70% of the total tissue volume ($\phi = 0.7$), then the predicted scattering coefficient based on the FDTD computed scattering cross section values in Fig. 5 falls between 60 and 105 cm^{-1}. These values of μ_s are similar to those of epithelial tissues [24] but are slightly underestimated because the internal structure of each organelle has not been taken into account.

The role of melanin in determining light distribution in tissues has been largely that of an absorber. However, in individual cells, its high index of refraction relative to the surrounding cell components causes a large increase in the scattering pattern, as demonstrated in Fig. 3. The absorption of the melanin granules can be accounted for in the FDTD simulations by assigning each granule a conductivity σ, although this has very little effect on the scattering patterns for cells with melanin since the pathlength is small. The large increase in high angle scatter has been observed in *in vivo* confocal [1] and OCT [25] images of the skin, which measure single scattering.

The calculated anisotropy factor, g, for a cell with organelles (Fig. 5) is higher than the values of g typically measured for tissues which lie in the range of 0.8–0.97 [24], [26] because the simulation calculates the scattering pattern for a single cell, whereas measurements typically involve tissue sections containing multiple cells as well as other tissue structures such as collagen and elastin. In addition, the organelles in this work were assumed to be homogeneous dielectric objects. Actual organelles are inhomogeneous with spatially varying dielectric properties that will cause an increase in the amount of scattered light. The FDTD method is able to account for this internal structure if it is known. Therefore, an understanding of the 3-D dielectric structure of cells is required for more accurate calculations. However, few detailed studies of the index of refraction of cells and organelles have been undertaken.

The FDTD method has large computational requirements for 3-D problems. The amount of storage and CPU time limits the method to single cell calculations at the present time. The computational requirements of scattering from cells in two dimensions using the FDTD technique [27] is considerably less than that of three dimensions, and multiple cells can be modeled. However, approximating cells as 2-D structures alters the shape of the phase functions. For example, the anisotropy value g, for a 3-D cell containing only a nucleus and cytoplasm was computed to be 0.99, while the two-dimensional (2-D) phase function of the same cell, computed by modeling a cross section of the 3-D cell, yields a value of 0.96. In a cell containing melanin, the values of g were 0.96 and 0.65 for 3-D and 2-D cells, respectively. However, the 2-D model [27] did exhibit the same general trends as the 3-D model—small organelles contributed more than the nucleus, and the anisotropy decreased with organelle volume fraction. Therefore, the 2-D approximation can be used to qualitatively predict the influence of organelles, but the 3-D model must be used to quantitatively compute scattering cross sections and anisotropy values of cells.

VI. Conclusion

The FDTD method has been applied to light scattering from cells containing different amounts of organelles. The FDTD method has advantages over the Mie theory since it accounts for multiple organelles within the cell simultaneously and is relatively easy to implement. The results showed that small organelles play a significant role in light scattering from cells, and the volume fraction of organelles affects both the total amount of scattered light and the angular distribution of scattered light. The results also demonstrate the need for more accurate measurements of the index of refraction of cells and cell components for more accurate determination of the scattering patterns.

References

[1] M. Rajadhyaksha, M. Grossman, D. Esterwitz, R. Webb, and R. Anderson, " *In-vivo* confocal scanning laser microscope of human skin: Melanin provides strong contrast," *J. Invest. Dermatol.*, vol. 104, pp. 946–952, 1995.

[2] D. Huang, E. Swanson, C. Lin, J. Schuman, W. Stinson, W. Chang, M. Hee, T. Flotte, K. Gregory, C. Puliafito, and J. Fujimoto, "Optical coherence tomography," *Science*, vol. 254, pp. 1178–81, Nov. 1991.

[3] D. Boas, M. O'Leary, B. Chance, and A. Yodh, "Scattering of diffuse photon density waves by spherical inhomogeneities within turbid media: Analytic solution and applications," in *Proc. National Academy Scis., USA*, 1994, vol. 91, pp. 4887–4891.

[4] E. Sevick, J. Frisoli, C. Burch, and J. Lakowicz, "Localization of absorbers on scattering media using frequency domain measurements of time-dependent photon migration," *Appl. Opt.*, vol. 33, pp. 3562–3570, 1994.

[5] I. Saidi, S. Jacques, and F. Kittel, "Mie and Rayleigh modeling of visible-light scattering in neonatal skin," *Appl. Opt.*, vol. 34, pp. 7410–7418, 1995.

[6] K. Yee, "Numerical solutions of initial boundary value problems involving Maxwell's equations in isotropic media," *IEEE Trans. Antennas Propagat.*, vol. AP-14, pp. 302–307, 1966.

[7] D. M. Sullivan, D. T. Borup, and O. P. Gandhi, "Use of the finite-difference time-domain method in calculating EM absorption in human tissues," *IEEE Trans. Biomed. Eng.*, vol. 34, pp. 148–157, 1987.

[8] A. Taflove and K. Umashankar, "Radar cross section of general three-dimensional structures," *IEEE Trans. Electromagn. Compat.*, vol. 25, pp. 433–440, 1983.

[9] R. Luebbers and H. Hunsberger, "FDTD for Nth-order dispersive media," *IEEE Trans. Antennas Propagat.*, vol. 40, pp. 1297–1301, 1992.

[10] K. Shlager and J. Schneider, "A selective survey of the finite-difference time-domain literature," *IEEE Antennas Propagat. Mag.*, vol. 37, pp. 39–56, 1995.

[11] A. Taflove and M. Brodwin, "Numerical solution of steady-state electromagnetic scattering problems using the time-dependent Maxwell's equations," *IEEE Trans. Microwave Theory Tech.*, vol. MTT-23, pp. 623–630, 1975.

[12] J. G. Blaschak and G. A. Kriegsmann, "A comparative study of absorbing boundary conditions," *J. Computat. Phys.*, vol. 77, pp. 109–139, 1988.

[13] G. Mur, "Absorbing boundary conditions for the finite-difference approximation of the time-domain electromagnetic-field equations," *IEEE Trans. Electromagn. Compat.*, vol. EMC-23, pp. 377–382, 1981.

[14] Z. P. Liao, H. L. Wong, B. P. Yang, and Y. F. Yuan, "A transmitting boundary for transient wave analysis," *Sci. Sin., Ser. A*, vol. 27, pp. 1063–1076, 1984.

[15] J.-P. Berenger, "A perfectly matched layer for the absorption of electromagnetic waves," *J. Computat. Phys.*, vol. 114, pp. 185–200, 1994.

[16] K. R. Umashankar and A. Taflove, "A novel method to analyze electromagnetic scattering of complex objects," *IEEE Trans. Electromagn. Compat.*, vol. 24, pp. 397–405, 1982.

[17] R. S. David and L. T. Wille, "Massively parallel finite-difference time-domain methods for electromagnetic scattering problems," in *Proc. 10th Annu. Rev. Progress Appl. Computational Electromagnetics*, Monterey, CA, Mar. 1994, vol. 1, pp. 495–502.

[18] R. Luebbers, S. Kunk, M. Schneider, and F. Hunsberger, "A finite-difference time-domain near zone to far zone transformation," *IEEE Trans. Antennas Propagat.*, vol. 39, pp. 429–433, 1991.

[19] C. M. Furse and O. P. Gandhi, "Why the DFT is faster than the FFT for FDTD time-to-frequency domain conversions," *IEEE Microwave Guided Wave Lett.*, vol. 5, no. 10, pp. 326–328, 1995.

[20] C. Balanis, *Advanced Engineering Electromagnetics*. New York: Wiley, 1989.

[21] L. G. Henyey and J. L. Greenstein, "Diffuse radiation in the galaxy," *Astrophys. J.*, vol. 93, pp. 70–83, 1941.

[22] J. Mourant, J. Boyer, A. Hielscher, and I. Bigio, "Influence of the scattering phase function on light transport measurements in turbid media performed with small source-detector separations," *Opt. Lett.*, vol. 21, pp. 546–548, 1996.

[23] A. Ishimaru, *Wave Propagation and Scattering in Random Media*, vol. 1. New York: Academic, 1978.

[24] W. Cheong, S. Prahl, and A. J. Welch, "A review of the optical properties of biological tissue," *IEEE J. Quantum Electron.*, vol. 26, pp. 2166–2185, 1990.

[25] V. Gelikonov, A. Sergeev, G. Gelikonov, and F. Feldchtein, "Characterization of human skin using optical coherence tomography," in *Proc. BiOS Europe*, Sept. 1996.

[26] S. Jacques, C. Alter, and S. Prahl, "Angular dependence of HeNe laser light scattering by human dermis," *Lasers Life Sci.*, vol. 1, pp. 309–333, 1987.

[27] A. Dunn, C. Smithpeter, A. J. Welch, and R. Richards-Kortum, "Light scattering from cells," in *OSA Tech. Dig.—Biomedical Optical Spectroscopy and Diagnostics*. Washington, DC: Opt. Soc. Amer., 1996, pp. 50–52.

[28] J. Maier, S. Walker, S. Fantini, M. Franceschini, and E. Gratton, "Possible correlation between blood glucose concentration and the

reduced scattering coefficient of tissues in the near infrared," *Opt. Lett.*, vol. 19, pp. 2062–2064, 1994.
[29] A. Brunsting and P. Mullaney, "Differential light scattering from spherical mammalian cells," *Biophys. J.*, vol. 14, pp. 439–453, 1974.
[30] H. Liu, B. Beauvoit, M. Kimura, and B. Chance, "Dependence of tissue optical properties on soluute-induced changes in refractive index and osmolarity," *J. Biomed. Opt.*, vol. 1, pp. 200–211, 1996.
[31] I. Vitkin, J. Woolsey, B. Wilson, and R. Anderson, "Optical and thermal characterization of natural (sepia oficinalis) melanin," *Photochem. Photobiol.*, vol. 59, pp. 455–462, 1994.

Andrew Dunn received the B.S. degree in physics from Bates College in Lewiston, ME, in 1992 and the M.S. degree in electrical engineering from Northeastern University, Boston, MA, in 1994. Currently he is pursuing the Ph.D. degree in biomedical engineering at the University of Texas at Austin.

His doctoral research involves developing an understanding of the physics of light scattering in tissue through numerical simulation and experimental measurements.

Rebecca Richards-Kortum received the B.S. degree in physics and mathematics with highest distinction from the University of Nebraska-Lincoln in 1985, the M.S. degree in physics and the Ph.D. degree in medical physics from the Massachusetts Institute of Technology, Cambridge, in 1987 and 1990, respectively.

In 1990, she joined the faculty as an Assistant Professor at the University of Texas at Austin, where she has established collaborative research projects which focus on the application of optical spectroscopy for detection of precancer and atherosclerosis.